Eur. Phys. J. D **40**, 51–56 (2006)
DOI: 10.1140/epjd/e2006-00131-2

THE EUROPEAN PHYSICAL JOURNAL D

Kinetic energy oscillations in annular regions of ultracold neutral plasmas

S. Laha[1,a], Y.C. Chen[2], P. Gupta[1], C.E. Simien[1], Y.N. Martinez[1], P.G. Mickelson[1], S.B. Nagel[1], and T.C. Killian[1]

[1] Department of Physics and Astronomy and Rice Quantum Institute, Rice University, Houston, Texas 77005, USA
[2] Institute of Atomic and Molecular Sciences Academia Sinica, P.O. Box 23-166, Taipei 106, Taiwan ROC

Received 2nd December 2005 / Received in final form 26 March 2006
Published online 15 June 2006 –

Abstract. A study of ion equilibration in annular regions of ultracold strontium plasmas is reported. Plasmas are formed by photoionizing laser-cooled atoms with a pulsed dye laser. The experimental probe is spatially-resolved absorption spectroscopy using the $^2S_{1/2}$–$^2P_{1/2}$ transition of the Sr^+ ion. The kinetic energy of the ions is calculated from the Doppler broadening of the spectrum, and it displays clear oscillations during the first microsecond after plasma formation. The oscillations, which are a characteristic of strong coulomb coupling, are fit with a simple phenomenological model incorporating damping and density variation in the plasma.

PACS. 52.35.-g Waves, oscillations, and instabilities in plasmas and intense beams – 32.80.Fb Photoionization of atoms and ions – 32.80.Pj Optical cooling of atoms; trapping

1 Introduction

In plasmas formed by photoionizing laser-cooled atoms [1], the ions have relatively low kinetic energy immediately after formation. However, their spatial distribution is uncorrelated and has a higher Coulombic potential energy than in thermodynamic equilibrium. As ions move to lower their potential energy, and spatial correlations develop, their kinetic energy increases. This phenomenon is called disorder induced heating and it was first predicted in [2] and observed experimentally in [3]. If the ions are initially uncorrelated and the ions interact through the screened Coulomb interaction, $U(r) = e^2 \exp(-\mathrm{r}/\lambda_D)/\mathrm{r}$, where $\lambda_D = \sqrt{\epsilon_0 k_B T_e/n_e e^2}$ is the electron Debye screening length, then the equilibrium temperature is given as [2]

$$T_i = \frac{2}{3}\frac{e^2}{4\pi\epsilon_0 a k_B}\left|\tilde{U}(\kappa,\Gamma_i) + \frac{\kappa(n_i,T_e)}{2}\right|. \qquad (1)$$

Here, T_e is the electron temperature, $n_e \simeq n_i$ is the density of electrons and ions respectively, $a = (3/4\pi n_i)^{1/3}$ is the inter particle distance, $\kappa = a/\lambda_D$, and $\Gamma_i = e^2/4\pi\epsilon_0 a k_B T_i$ is the coulomb coupling parameter for the ions. $\tilde{U}$, the excess potential energy per particle in units of $e^2/4\pi\epsilon_0 a$, is tabulated in [4] using a molecular dynamics simulation. Equation (1) was confirmed experimentally in [5].

It was also shown in [5] that the kinetic energy of the ions undergoes damped oscillation during equilibration. Such oscillations of strongly coupled plasmas had previously been seen in computer simulations [6–10]. Physically one expects oscillations to occur at the ion plasma frequency, $\omega_{pi} = \sqrt{n_i e^2/m_i\epsilon_0}$, where m_i is ion mass. For a typical density of 10^{16} m^{-3}, $2\pi/\omega_{pi} \simeq 600$ ns.

Initially, the evolution of the kinetic energy of all the ions is synchronized in time, but there is no long range spatial coherence to the motion because the ions are moving in random directions. Although we must be cautious in ascribing the oscillation to an ion collective mode, we can gain intuition from the dispersion relation for electrostatic wave propagation in a two component plasma [11],

$$1 - \frac{\omega_{pe}^2}{\omega^2 - k^2 v_e^2} - \frac{\omega_{pi}^2}{\omega^2 - k^2 v_i^2} = 0, \qquad (2)$$

where, $k = 2\pi/\lambda$ is the wave vector and $v_{e,i} \simeq \sqrt{k_B T_{e,i}/m_{e,i}}$ are the electron or ion thermal velocities. Assuming that $\omega \ll \omega_{pe}$ and $T_e \gg T_i$, which results in the approximation $v_i \ll \omega/k \ll v_e$, the dispersion relation implies,

$$\omega = \omega_{pi}\sqrt{\frac{k^2\lambda_D^2}{1+k^2\lambda_D^2}}. \qquad (3)$$

Ion oscillations are on a length scale of approximately an inter particle distance. If we were to assign a wave vector to the ion motion observed here, it would be $k \simeq 2\pi/a \gg 1/\lambda_D$ and in this regime, $\omega = \omega_{pi}$.

The ion-density varies over space and consequently, ω_{pi} varies with position. This causes the oscillations to

[a] e-mail: sampad@rice.edu

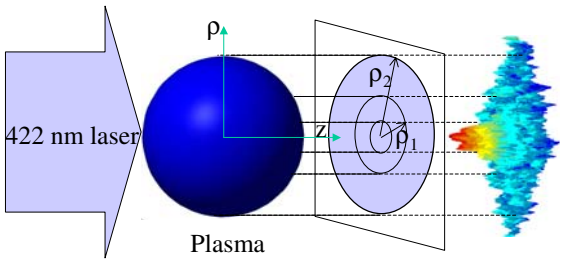

Fig. 1. (Color online) Spatially-resolved absorption imaging. The plasma-image is divided into three annular regions such that each contains an equal number of ions. An experimental optical depth is shown to the right.

dephase, which complicates their study. To circumvent this problem, we divide the analysis of the plasma into concentric cylinders-each having the same number of ions and less density variation than the entire cloud. In the annular regions, plasma oscillations are prominent and easier to analyze.

2 Creating and absorption-imaging Sr plasma

To produce ultracold neutral plasma, Sr atoms are cooled in a magneto-optical trap (MOT) [12] on the $^1S_0$–$^1P_1$ dipole allowed transition at 461 nm. Roughly 2×10^8 atoms are trapped at a temperature of about 10 mK. The atom density has a Gaussian distribution over space, $n(r) = n_0 \exp\left(-r^2/2\sigma^2\right)$, with $\sigma \simeq 10^{-3}$ m and peak density, $n_0 \simeq 10^{16}$ m^{-3} [3]. The MOT is then turned off, and a laser resonant with the cooling transition illuminates the cloud for 1 μs to increase the population in the $^1P_1$ level. The atoms in the $^1P_1$ state are photoionized with a 10 ns pulse from a dye laser whose wavelength is tuned to an energy E_e above the ionization continuum. Because of the small electron-to-ion mass ratio, nearly all the energy of the photon above the ionization threshold is transferred to the electron kinetic energy [1]. E_e/k_B can be as low as 100 mK which is the bandwidth of laser.

We probe the plasma using absorption imaging on the 422 nm $^2S_{1/2}$–$^2P_{1/2}$ transition in the ions [3]. As shown in Figure 1, the laser passes through the trapping region and falls on an intensified CCD camera. The optical depth of the medium is given by $OD(x,y) = \ln(I_{background}/I_{plasma})$, where I_{plasma} and $I_{background}$ are the intensity of the transmitted laser when the plasma is present and when it is not. The optical depth can be related to physical quantities through

$$OD(x,y) = \int_{-\infty}^{\infty} n_i(\boldsymbol{r})\alpha\left(\nu,\boldsymbol{r}\right) dz, \qquad (4)$$

where $\alpha(\nu,\boldsymbol{r})$ is the absorption cross-section of the ions at a probe laser frequency ν. The cross-section varies with position because the kinetic energy, which produces Doppler broadening, varies. From this point onwards we drop the subscript i, and all quantities refer to ion properties unless otherwise specified.

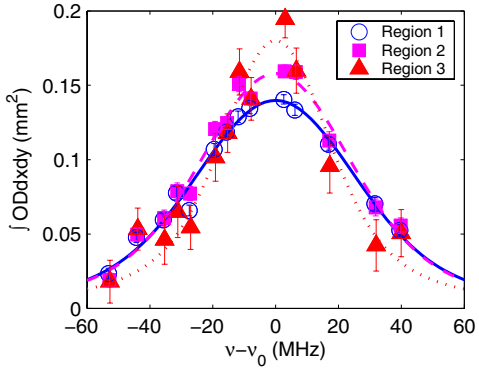

Fig. 2. (Color online) Spectra of the three annular regions. The lines show Voigt fits to the spectra. The above image was taken at 192 ns after photoionization, for $n_0 = 9.5\times10^{14}$ m^{-3} and initial electron kinetic energy, $E_e/k_B = 55.5$ K.

To study oscillations, we divide the plasma image into three annular regions of equal number of ions (Fig. 1). If ρ denotes the radial coordinate in a cylindrical system, then this division gives us three regions given by $(\rho_1,\rho_2) = (0, 0.9\sigma), (0.9\sigma, 1.48\sigma), (1.48\sigma, \infty)$. We will call these regions as region 1, region 2 and region 3 respectively. We can sum the OD over the region to get the absorption spectrum $S_{reg}(\nu)$ for each region as

$$S_{reg}(\nu) \equiv \int_{A_{reg}} OD(x,y)dxdy = \int_{V_{reg}} n(\boldsymbol{r})\alpha\left(\nu,\boldsymbol{r}\right) d^3r \quad (5)$$

where, the spatial integration is over each annular region, A_{reg}. Typical spectra of the three annular regions are shown in Figure 2. Note that the spectrum of the center region is widest and that of the outermost is narrowest. This happens because the width of the spectrum is a measure of kinetic energy of the plasma, and disorder induced heating increases with ion density. The area of each curve is approximately equal because $\int S_{reg}(\nu)d\nu \propto N_{reg}$ is the same for all the regions, where N_{reg} is the number of ions in each region.

To quantitatively analyze the spectra, we introduce a full expression for the absorption cross-section, α. The natural linewidth of the transition, $\gamma_0 = 2\pi \times 20.21 \times 10^6$ s^{-1}, and the laser linewidth, $\gamma_{laser} = 2\pi \times (5 \pm 2) \times 10^6$ s^{-1}, set a minimum width to the spectrum. Ion motion along the direction of the laser beam contributes Doppler broadening. A convolution of these effects yields

$$S_{reg}(\nu) = \frac{3^*\lambda^2}{2\pi}\frac{\gamma_0}{\gamma_{eff}} \int_{-\infty}^{\infty} ds \frac{1}{1+\left[\frac{2(\nu-s)}{\gamma_{eff}/2\pi}\right]^2} \times \int_{V_{reg}} \frac{d^3r\, n(\boldsymbol{r})}{\sqrt{2\pi}\sigma_D[T_{thermal}(\boldsymbol{r})]} \exp\left\{-\frac{[s-\nu_0-\delta\nu(z)]^2}{2\sigma_D^2[T_{thermal}(\boldsymbol{r})]}\right\}. \qquad (6)$$

The factor 3^* accounts for the laser and ion polarization [13]. In our case, $3^* = 1$ due to the random alignment of ions and linear polarization of the laser. Here,

$\lambda = 422$ nm is the transition wavelength, $\gamma_{eff} = \gamma_0 + \gamma_{laser}$ and ν_0 is the resonance frequency of the transition. The exponential Doppler term describes broadening due to random motion and directed plasma expansion. Whether the system has reached local thermal equilibrium or not, we characterize the kinetic energy arising from random motion by a temperature $T_{thermal}$ that may vary with position, and a Doppler width $\sigma_D[T_{thermal}(r)] = (1/\lambda)\sqrt{k_B T_{thermal}(r)/m}$. Directed expansion of the plasma [3,14–18] is driven by the kinetic energy of the electrons, which exerts a radial pressure on the ions. The expansion velocity as a function of time and position, including effects of adiabatic electron cooling, is given in [14,16,19]. The Doppler shift of the resonant frequency due to the expansion velocity of ions is given by [17]

$$\delta\nu(z) = \frac{v_z}{\lambda} = \frac{z k_B T_e t}{m_i(\sigma^2 + \frac{k_B T_e t^2}{m})\lambda}. \quad (7)$$

Here, v_z is the local average velocity along the laser direction, which only arises from radial expansion, z is the distance from the center of the cloud along the direction of the laser, and t is the time since photoionization. The second term in parenthesis in equation (7) accounts for electron cooling and is small for the data discussed here.

The integral over volume in equation (6) complicates the expression. Fortunately, we can simplify it as

$$S_{reg}(\nu) = \frac{3^*\lambda^2}{2\pi}\frac{\gamma_0}{\gamma_{eff}}\frac{N_{reg}}{\sqrt{2\pi}\tilde{\sigma}_{D,reg}}\int_{-\infty}^{\infty} ds \frac{1}{1+\left[\frac{2(\nu-s)}{\gamma_{eff}/2\pi}\right]^2} \times \exp\left[-\frac{(s-\nu_0)^2}{2\tilde{\sigma}^2_{D,\mathrm{reg}}}\right], \quad (8)$$

where $\tilde{\sigma}_{D,reg} = (1/\lambda)\sqrt{k_B T_{eff,reg}/m}$, with $T_{eff,reg}$ being an effective ion temperature of the region parameterizing all Doppler broadening from random motion and expansion. This approximation is possible because the kinetic energy distribution during the expansion stays close to Gaussian, even though the velocities do not represent random motion in thermal equilibrium. Numerical simulations testing the accuracy of this approximation are shown in Figure 3, and they are explained in detail in the following section. Fits of the data to this simple Voigt profile are shown in Figure 2.

3 Phenomenological descriptions of the effective temperature

The main quantity we extract from each spectrum is $T_{eff,reg}$. It clearly describes Doppler broadening, but how do we relate it to underlying physical parameters of the plasma? For each annular region and over a wide range of conditions of local thermal equilibrium (LTE), numerical calculations of the full integral (Eq. (6)), show that $T_{eff,reg}$ can be related to the average of the kinetic energy

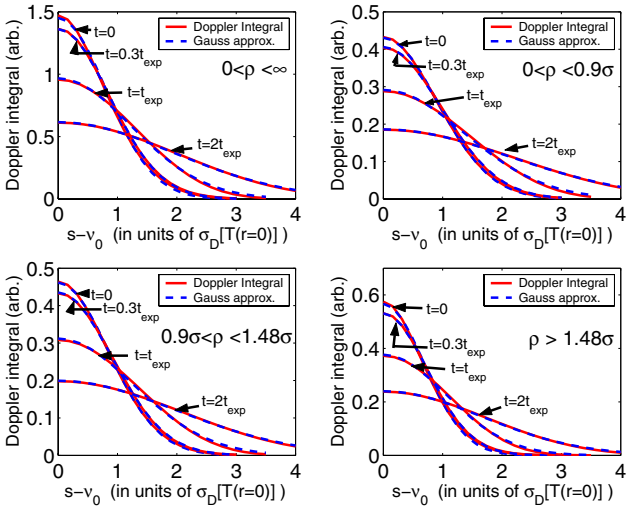

Fig. 3. (Color online) Numerical simulation showing that for annular regions and local thermal equilibrium given by equation (1), the spatial integral of the density times the Doppler profile in equation (6) can be replaced by a simple Gaussian with an effective temperature given by equation (9). Notice that as t increases, so does the Doppler width. The analysis takes the electronic screening effects into consideration and this specific result is for $n_0 = 9 \times 10^{15}$ m^{-3} and $T_e = 30$ K. In the figure, the continuous line is the density average of Doppler profile, and the dashed line is the approximated Gaussian curve. (In the above figure, the analysis for the whole volume, $0 < \rho < \infty$, was presented in [17] and it is shown here just for comparison.)

from random motion, $k_B \times \langle T_{thermal}(r)\rangle_{reg}$, by

$$T_{eff,reg} = \langle T_{thermal}(r)\rangle_{reg}\left[C + (t/t_{exp})^2\right]. \quad (9)$$

This was demonstrated for analysis of the entire plasma in [17]. Here we extend the treatment to annular regions.

By the time the kinetic energy due to expansion becomes significant, the oscillations have largely damped out and the plasma has reached LTE. This allows us to define

$$t_{exp} = \frac{\sigma}{T_e}\sqrt{\frac{m_i\langle T_{thermal}(r)\rangle}{k_B}} \quad (10)$$

as the characteristic time in which ions develop enough radial expansion velocity so that the Doppler broadening due to expansion is equal to the thermal Doppler broadening. The average is taken after LTE is reached, so one can think of $K_B\langle T_{thermal}(r)\rangle$ as a measure of kinetic energy coming from disorder-induced heating given by equation (1). For numerical checks of equation (9), however, we will let $T_{thermal}(r)$ take various forms. For global thermal equilibrium of the ions ($T_{thermal}(r) =$ constant), equation (9) results from a trivial analytic evaluation of equation (6) and $C = 1$. If we assume LTE at a temperature given by equation (1)[1], for peak densities

[1] For a given peak density, n_0, and electron temperature, T_e, we can solve equation (1) by iterative method and obtain a distribution of the ionic temperature T_i.

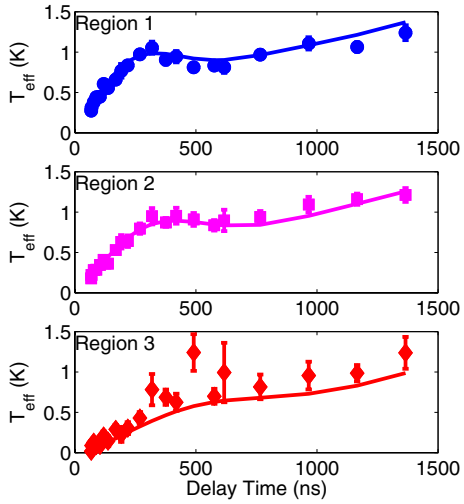

Fig. 4. Variation of the effective temperature, $T_{eff,reg}$ with delay time for $n_0 = 1.5 \times 10^{15}\,\mathrm{m}^{-3}$ and initial electron kinetic energy, $E_e/k_B = 55.5\,\mathrm{K}$. The marker points are the raw data and the continuous curve is the fit of the effective ion temperature of different regions to the oscillation function (Eq. (12)). For this data, $\chi^2_\nu = 1.5$ with 56 degrees of freedom.

of 10^{14}–5×10^{16} m^{-3} and initial electron temperatures of 1–1000 K, the values of C are 0.94 ± 0.04, 0.98 ± 0.01, 0.98 ± 0.02 and 0.94 ± 0.04 for whole volume, region 1, region 2 and region 3 respectively. The result of the numerical simulation is shown in Figure 3. This is the situation we expect in our system for data presented here and times after the oscillations have damped. When the system is not in LTE, we will still assume the form of equation (9) and these values of C in our analysis, but we can only claim an approximate quantitative relationship of $T_{eff,reg}$ to underlying physical parameters. Perhaps more detailed simulations [14] can remove this limitation.

Figure 4 shows the ion effective temperature at different delay times and for different regions. There is a clear indication of temperature oscillations in early delay times. The oscillation period is smallest in the innermost region and largest in the outermost region. This is because the time scale is equal to $2\pi/\omega_{pi}(r)$ and $\omega_{pi}(r) \propto \sqrt{n_i(r)}$. Also, the equilibration temperature of the ions after oscillations damp is highest for the innermost region and lowest for the outermost region. This can be explained from the fact that the LTE temperature (T_i) is proportional to $e^2/4\pi\epsilon_0 a k_B$ and $a(r) \propto [n_i(r)]^{-1/3}$.

We can gain much insight into kinetic energy oscillations with a a phenomenological model for $T_{thermal}(r)$, which we use to describe kinetic energy due to oscillations and thermal motions. If we assume each ion's velocity varies as $v_0 \sin\omega_{pi}t$ [9,10], where, ω_{pi} is the local ion plasma frequency, then $T_{thermal} \propto v^2 = v_0^2 \sin^2\omega_{pi}t$. If we allow for damping of the oscillations by a damping parameter ζ, and equilibration at T_i from equation (1), then,

$$T_{thermal}(r,t) = T_i(r)\left[1 - \cos(2\omega_{pi}t)e^{-\zeta\omega_{pi}t}\right]. \qquad (11)$$

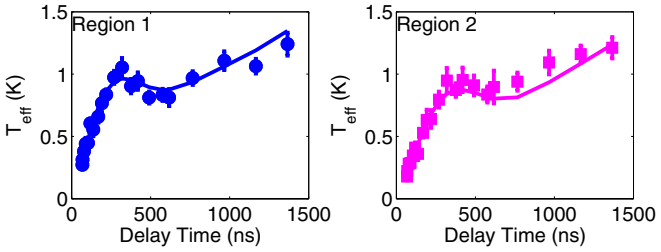

Fig. 5. These fits show the fits of the ion temperature of different regions to the oscillation function (Eq. (12)) when only region 1 and region 2 are fitted. The χ^2_ν is very close to unity and it indicates that the fitting-function is actually a good representation of our experimental data. For this data, $\chi^2_\nu = 1.2$ with 36 degrees of freedom.

We average equation (11) over the volume of the region and assume the effect of expansion is well-described by equation (9) at all times to obtain the model effective temperature as

$$T_{eff,reg}(t) = \int_{\rho_1}^{\rho_2} d\rho \int_{-\infty}^{\infty} dz\; 2\pi\rho \frac{n_0 e^{-r^2/2\sigma_i^2}}{N_{reg}} T_i(r)$$
$$\times \left\{1 - \cos\left[2\omega_{pi}(r)t\right] e^{-\zeta\omega_{pi}(r)t}\right\} \left[C + \left(\frac{t}{t_{exp}}\right)^2\right], \qquad (12)$$

where we have used cylindrical coordinates with ρ_1 and ρ_2 indicating the cylindrical boundary of the annular regions and $r^2 = \rho^2 + z^2$. It should be noted here that the locally equilibrated temperature, $T_i(r)$ is a function of position because in equation (1) the density is a function of position. Also, the expansion time t_{exp} in the above expression is a constant of the plasma and is independent of the regional boundaries. A numerical verification of this fact is given in [20].

To fit the spatial and temporal variation of the ion kinetic energy to equation (12), as shown in Figure 5, we varied n_0, T_e, σ and ζ. Variation of σ is equivalent to variation of t_{exp}, since we use equation (10) for t_{exp} and use equation (1) to set $\langle T_{thermal}(r)\rangle = \langle T_i(r)\rangle$. The average is over the entire plasma. All the parameters except ζ were the same for all regions. The fitting was done by the method of least squares, in which the reduced χ^2 is minimized. Initially we fit all three annular regions. An example is shown in Figure 4. The quantities, n_0, σ, and to some extent T_e, are also controlled experimentally. We will compare the fit results with values determined independently to check the phenomenological model. In total, eight different sets of data were fit, each having experimentally set values of E_e/k_B varying from 16.5 K to 84 K and n_0 between 1.5×10^{15} and 9.5×10^{15} m^{-3}.

The one-sigma errors of the optimal parameters from the fits were on the order of 10% of the parameter's value. Ideally, the value of χ^2_ν should be equal to 1 for a good fit but the value of χ^2_ν averaged 1.5 for a typical number of degrees of freedom of about 90 which is unreasonably high.

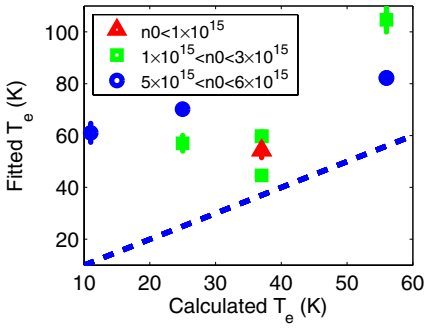

Fig. 6. Comparing fit values of T_e with values calculated from equation (13). The dashed line is drawn for easier comparison. Notice that the fit values of T_e are higher than the calculated ones. Statistical uncertainties are typically smaller than the size of the symbols. There is a systematic uncertainty of ± 5 K in the calculated T_e due to calibration of the dye laser wavelength. (The density values in the legend are calculated from the ion-image.)

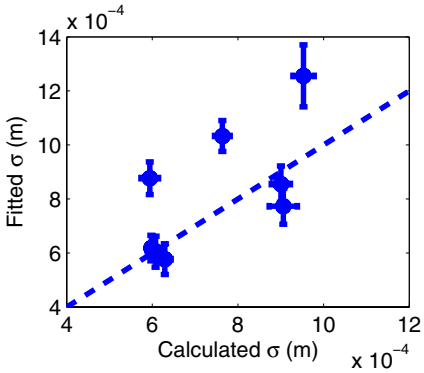

Fig. 7. Comparison of ion cloud size, σ_i, taken from the oscillation fit (Eq. (12)) and values calculated directly from the plasma image. The dashed line is drawn for easier comparison. Error bars represent statistical uncertainty, and there is a 20% scale uncertainty in the calculated value, as described in the text.

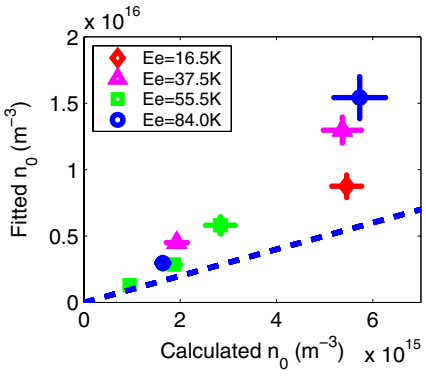

Fig. 8. Comparison of values of n_0 taken from the oscillation fit (Eq. (12)) and values calculated directly from the plasma image. The dashed line is drawn for easier comparison. Error bars represent statistical uncertainty, and there is a 60% scale uncertainty in the calculated value, as described in the text. The electron energy calculated from the ionizing laser frequency is shown in the legend.

This discrepancy led us to closely examine the fits and we found that the fitted $T_{eff,reg}$ in region 3 is systematically lower than the experimental $T_{eff,reg}$ for all the data sets, and the residuals in region 3 contribute the most to the high values of χ^2_ν. One explanation might be that the outer region is not perfectly neutral because high energy electrons have escaped from this region [1]. The theoretical model that we use assumes neutrality of the plasma. A shortage of electrons would imply less screening and a higher ion temperature after equilibrium. When we omitted the outer region from the fit as shown in Figure 5, χ^2_ν averaged 1.2 which is more reasonable. This suggests that our fitting-function is a good representation of our experimental data in regions 1 and 2, but neglects essential physics important in region 3. All following results are from the fitting of region 1 and 2 only.

We also note that even fitting just regions 1 and 2, the parameters are strongly overdetermined. Most importantly, the oscillation frequency and equilibrium temperature are both determined by the density, and they both fit quite well.

To check systematics, we compare quantities obtained from the fitting (n_0, T_e and σ) with their values obtained from other independent techniques. For example, the initial electron temperature can be calculated using the formula

$$\frac{3}{2}k_B T_e = E_e = h\nu_{laser} - \Phi_{IP}, \qquad (13)$$

where, ν_{laser} is the frequency of the photoionizing laser, and $\Phi_{IP} = 4.819 \times 10^{-19}$ J is the ionization potential of the $^1P_1$ level of strontium. Figure 6 shows a comparison of the fitted and the calculated T_e. As can be seen from the figure, the values of fitted T_e are higher than the calculated ones. This happens because electrons heat above the temperature given by equation (13) due to three-body recombination [16], disorder-induced heating [21] and continuum lowering [22]. Our analysis gives us good method to measure this heating, which can be a subject of future study.

The size and peak density of the plasma can also be calculated directly from the plasma image. Since we image along only one axis, the information for the third dimension can not be very well determined. This puts a conservative errorbar of 20% on our size values, and 60% on the peak density. Conditions are stable during the experiment, so these represent systematic uncertainty, not random error. Comparisons between values of σ taken from the oscillation fit (Eq. (12)) and values calculated directly from the plasma image are shown in Figure 7 and they agree reasonably well in light of the errorbars discussed above. A similar plot for n_0 (Fig. 8) shows that the values obtained from the fit significantly exceed the values obtained directly from the image. Investigating this discrepancy will be the subject of future study.

In our oscillation model, we also account for the damping of the oscillation. We don't know the exact cause of this damping but it might relate to ion-ion and

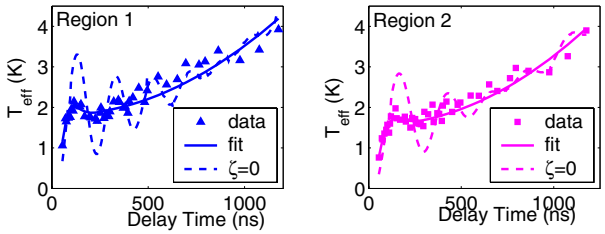

Fig. 9. Plot showing effect of damping on oscillations for $n_0 = 5.7 \times 10^{15}\,\mathrm{m}^{-3}$ and initial electron kinetic energy, $E_e/k_B = 84\,\mathrm{K}$. The dashed curve is a plot neglecting damping ($\zeta = 0$) and the continuous curve takes the effect of damping ($\zeta = 1.35$ for region 1 and $\zeta = 1.38$ for region 2) into account.

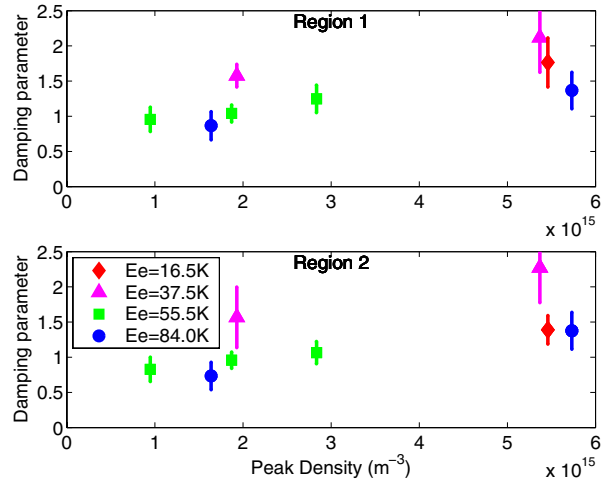

Fig. 10. Plots of damping parameter, ζ, versus the calculated peak density. Fits values of ζ are close to unity, in agreement with simulations [23]. The electron energy calculated from the ionizing laser frequency is shown in the legend.

ion-electron collisions or simply the scrambling of the oscillatory motion as ions move in the liquid-like medium [3,6].

Dephasing due to density variation within each region is not the main cause of apparent damping, as seen clearly in Figure 9. The dashed curve in the figure is a plot neglecting damping ($\zeta = 0$) and it does not fit the data well. The continuous curve takes damping into account. The damping was also observed in [6,7,23] where, a hybrid molecular dynamics approach was used to model equilibrating, strongly-coupled plasmas.

A plot of the damping parameter, ζ versus the calculated n_0 in Figure 10 shows that ζ has values around 1. The value of ζ is also observed to be 1 in the simulations of [23]. Although, we also see a slight increase in the damping parameter with high density and low initial electron energy.

4 Conclusions

To summarize, we have successfully shown the presence of kinetic energy oscillations in ultracold plasmas with frequency equal to the ion plasma frequency. Oscillations were previously seen in [5]. Here, we have provided details of a spatially-resolved analysis that increases their visibility. We also fit a phenomenological model to the effective temperature that accounts for density inhomogeneity and damping. This gives us deeper insight into the spatial and temporal dependence of the kinetic energy oscillations.

We thank the Office of Fusion Energy Sciences of the Department of Energy, National Science Foundation (Grant #PHY-0355069), Research Corporation, Alfred P. Sloan Foundation, and David and Lucile Packard Foundation for funding this research.

References

1. T.C. Killian, S. Kulin, S.D. Bergeson, L.A. Orozco, C. Orzel, S.L. Rolston, Phys. Rev. Lett. **83**, 4776 (1999)
2. M.S. Murillo, Phys. Rev. Lett. **87**, 115003 (2001)
3. C.E. Simien, Y.C. Chen, P. Gupta, S. Laha, Y.N. Martinez, P.G. Mickelson, S.B. Nagel, T.C. Killian, Phys. Rev. Lett. **92**, 143001 (2004)
4. S. Hamaguchi, R.T. Farouki, D.H.E. Dubin, Phys. Rev. E **56**, 4671 (1997)
5. Y.C. Chen, C.E. Simien, S. Laha, P. Gupta, Y.N. Martinez, P.G. Mickelson, S.B. Nagel, T.C. Killian, Phys. Rev. Lett. **93**, 265003 (2004)
6. G. Zwicknagel, Contrib. Plasma Phys. **39**, 155 (1999)
7. I.V. Morozov, G.E. Norman, J. Phys. A: Mah. Gen. **36**, 6005 (2003)
8. T. Pohl, T. Pattard, J.M. Rost, J. Phys. B: At. Mol. Opt. Phys. **37**, 183 (2004)
9. H. Gould, G.F. Mazenko, Phys. Rev. Lett. **35**, 1455 (1975)
10. J.P. Hansen, E.L. Pollock, I.R. McDonald, Phys. Rev. Lett. **32**, 277 (1974)
11. W.D. Jones, H.J. Doucet, J.M. Buzzi, *An introduction to the linear theories and methods of electrostatic waves in plasmas* (Plenum Press, New York, 1985)
12. S.B. Nagel, C.E. Simien, S. Laha, P. Gupta, V.S. Ashoka, T.C. Killian, Phys. Rev. A **67**, 011401 (2003)
13. A.E. Siegman, *Lasers* (University Science Books, Sausolito, California, 1986)
14. T. Pohl, T. Pattard, J.M. Rost, Phys. Rev. Lett. **92**, 155003 (2004)
15. S. Kulin, T.C. Killian, S.D. Bergeson, S.L. Rolston, Phys. Rev. Lett. **85**, 318 (2000)
16. F. Robicheaux, J.D. Hanson, Phys. Plasmas **10**, 2217 (2003)
17. T.C. Killian, Y.C. Chen, P. Gupta, S. Laha, Y.N. Martinez, P.G. Mickelson, S.B. Nagel, A.D. Saenz, C.E. Simien, J. Phys. B **38**, 351 (2005), the RHS of equation (7) in [17] needs to be multiplied by a factor of γ_0/γ_{eff}
18. E.A. Cummings, J.E. Daily, D.S. Durfee, S.D. Bergeson, Phys. Rev. Lett. **95**, 235001 (2005)
19. E.A. Cummings, J.E. Daily, D.S. Durfee, S.D. Bergeson, Phys. Plasmas **12**, 123501 (2005)
20. S. Laha, Master's thesis, Rice University (2005)
21. S.G. Kuzmin, T.M. O'Neil, Phys. Plasmas **9**, 3743 (2002)
22. S. Mazevet, L.A. Collins, J.D. Kress, Phys. Rev. Lett. **88**, 55001 (2002)
23. T. Pohl, T. Pattard, J. Phys. Conf. Ser. **11**, 223 (2005)